Distribution of Husimi zeros in polygonal billiards

Debabrata Biswas*
Theoretical Physics Division, Bhabha Atomic Research Centre, Trombay, Mumbai 400 085, India

Sudeshna Sinha†
The Institute of Mathematical Sciences, CIT Campus, Taramani, Chennai 600 113, India

(Received 15 July 1998; revised manuscript received 4 January 1999)

The zeros of the Husimi function provide a minimal description of individual quantum eigenstates and their distribution is of considerable interest. We provide here a numerical study for pseudointegrable billiards which suggests that the zeros tend to diffuse over phase space in a manner reminiscent of chaotic systems but nevertheless contain a subtle signature of pseudointegrability. We also find that the zeros depend sensitively on the position and momentum uncertainties (Δq and Δp, respectively) with the classical correspondence best when $\Delta q = \Delta p = \sqrt{\hbar/2}$. Finally, short-range correlations seem to be well described by the Ginibre ensemble of complex matrices. [S1063-651X(99)03507-2]

PACS number(s): 05.45.−a, 03.65.Sq

I. INTRODUCTION

This paper deals with phase space parameterizations of one-dimensional *billiard map* eigenfunctions for polygonal enclosures. Specifically, we shall deal with the Bargman-Husimi representation and study the distribution of its zeros for regular, irregular, and bouncing ball modes. Such a study has been carried out before for integrable and chaotic billiards [1,2], and these systems are now reasonably well understood in the sense that the distribution reflects a correspondence with the underlying classical dynamics. As with most other objects of interest in generic polygonal (pseudointegrable) billiards, the distribution of zeros is interesting if only to explore the existence of such a correspondence with the classical system.

Of all possible Hamiltonian systems, billiards are perhaps the best understood category and exhibit the entire gamut of classical dynamics depending on the shape of the enclosure. Of these, polygonal billiards form an important subcategory, and apart from the rectangle and the triangles $(\pi/3,\pi/3,\pi/3)$, $(\pi/2,\pi/3,\pi/6)$, $(\pi/2,\pi/4,\pi/4)$, all other polygonal enclosures are nonintegrable [3]. Further, the ones with rational interior angles are pseudointegrable; they have two constants of motion as in integrable systems and yet their invariant surface in phase space has a genus $g>1$. One of the simplest examples of a pseudointegrable system is the $\pi/3$ enclosure for which $g=2$; *i.e., the invariant surface is a double torus*. Here, as in other pseudointegrable billiards, an initial (parallel) beam of trajectories splits after successive encounters with the $2\pi/3$ (in general $m\pi/n, m>1$) vertex and traverse different paths.

There are several important consequences of pseudointegrability at the classical level that are now known. However, as far as semiclassics is concerned, pseudointegrable billiards are still rather poorly understood. When the dynamics is integrable, an Einstein-Brillouin-Keller ansatz for the wave function [4]

$$\psi(q) \sim \sum_{j=1}^{N} A_j \exp(iS_j/\hbar) \tag{1}$$

works well at least in the limit $\hbar \to 0$. In the above, S_j are the (finitely many) branches of the classical action at energy E and A_j are constant amplitudes for integrable polygons. Such an ansatz, however, does not work for pseudointegrable billiards even though the number of sheets that constitute the invariant surface is still finite. We shall not discuss the reasons for its breakdown here but merely remark that no definite behavior for pseudointegrable eigenfunctions is known. For classically chaotic systems, on the other hand, the Schnirelman theorem [5] (suitable phase-space measures constructed from the eigenfunctions must tend towards the classical phase-space ergodic measure as $\hbar \to 0$) does provide a semiclassical constraint, albeit in a measure theoretic sense. Besides, there exist results on the amplitude distribution and spatial correlation function which have been subject to tests [6].

Despite the absence of any such result for pseudointegrable polygons, numerical studies [7] such as those for the amplitude distribution or nodal plots suggest that typical eigenfunctions are irregular and, broadly speaking, there is little to distinguish them from the eigenfunctions in chaotic systems. In the present paper, we shall try to refine this existing body of knowledge and will employ for this purpose a phase-space representation of quantum mechanics, which is known to highlight certain semiclassical features for integrable and chaotic systems. Our results are empirical, based on extensive numerical studies, and can be simply expressed as follows: the eigenfunctions of polygonal billiards as viewed in the Husimi representation tend to be irregular *but nevertheless contain a subtle signature of classical pseudointegrability*.

The paper is organized along the following lines. In Sec. II, we briefly review the Husimi-Bargman representations and the results on random analytic functions. We introduce the systems that we shall study and the quantum map under consideration in Sec. III. This is followed by our numerical

*Electronic address: dbiswas@apsara.barc.ernet.in
†Electronic address: sudeshna@imsc.ernet.in

results on the Husmini function and the density of zeros in Sec. IV. Finally, correlations are discussed in Sec. V and our conclusions are summarized in Sec. VI.

II. PHASE SPACE REPRESENTATIONS

Phase-space representations of quantum wave functions are best suited in semiclassical studies since the quantum dynamics (Heisenberg equation) then appears as an explicit deformation of the classical dynamics (Liouville equation) by shifting the analysis onto the density operator $\hat{\rho} = |\psi\rangle\langle\psi|$. In quantum mechanics, however, the phase-space representation of a state is not unique since operators $(\hat{q},\hat{p}$, for instance) may be ordered in various ways while having the same classical analog. A general expression for a quasiprobability distribution function may be expressed as [8]

$$\rho_{(\Omega)}(q,p,t) = \frac{1}{(2\pi)^2}\int d^2\xi \; e^{i(\xi^* z^* + \xi z)\hbar}\mathrm{Tr}[\Omega\{e^{-i\xi^*\hat{a}^\dagger}e^{-i\xi\hat{a}}\}\hat{\rho}], \tag{2}$$

where Ω refers to the ordering that is chosen. The Wigner distribution follows from a symmetric ordering of $(\hat{q},\hat{p})$ which implies

$$\Omega\{e^{-i\xi^*\hat{a}^\dagger}e^{-i\xi\hat{a}}\} = e^{-i\xi^*\hat{a}^\dagger - i\xi\hat{a}}, \tag{3}$$

while the Husimi function is a result of antinormal ordering:

$$\Omega\{e^{-i\xi^*\hat{a}^\dagger}e^{-i\xi\hat{a}}\} = e^{-i\xi\hat{a}}e^{-i\xi^*\hat{a}^\dagger}. \tag{4}$$

Using Eqs. (2) and (3), the distribution function in the Wigner representation, $\rho_w(q,p;\hbar)$, for a pure state can be explicitly written as

$$\rho_w(q,p;\hbar) = \frac{1}{(2\pi\hbar)^d}\int \langle q-\eta/2|\psi\rangle\langle\psi|q+\eta/2\rangle e^{ip\cdot\eta/\hbar}d\eta, \tag{5}$$

where d is the degree of freedom of a dynamical system. Thus, the expectation of a dynamical variable $\hat{A}$ is represented as

$$\mathrm{Tr}[\hat{A}|\psi\rangle\langle\psi|] = \int A_w(q,p)\rho_w(q,p)dqdp, \tag{6}$$

where

$$A_w(q,p) = \int \langle q-\eta/2|\hat{A}|q+\eta/2\rangle e^{ip\cdot\eta/\hbar}d\eta. \tag{7}$$

The Wigner function, however, takes positive as well as *negative* values and oscillates violently with a wavelength $\hbar$ in phase space. A coarse-grained distribution function is thus preferred and the Husimi function

$$\rho_h(q,p;\hbar) = \frac{1}{(\pi\hbar)^d}\int \rho_w(q',p';\hbar)\exp\left(-\sum_{i=1}^{N}\left[\frac{(q_i-q_i')^2}{2(\Delta q_i)^2} + \frac{(p_i-p_i')^2}{2(\Delta p_i)^2}\right]\right)dp'dq' \tag{8}$$

is one such example which can be expressed as a smoothened Wigner function. In this case, the smoothening is achieved through the Gaussian centred at a phase-space point (q,p). In Eq. (8) above,

$$\Delta q_i = \sqrt{\frac{\hbar}{2}}\sigma_i, \quad \Delta p_i = \sqrt{\frac{\hbar}{2}}\frac{1}{\sigma_i} \tag{9}$$

are the uncertainties in q and p, respectively. Note that ρ_h is merely a minimum-uncertainty (MU) state decomposition of the wave function ψ and can be expressed as

$$\rho_h(q,p;\hbar) = \frac{|\langle z|\psi\rangle|^2}{2\pi\hbar}, \tag{10}$$

where

$$|z\rangle = e^{-|z|^2/2}\sum_{n=0}^{\infty}\frac{z^n}{\sqrt{n!}}|n\rangle. \tag{11}$$

$\{|n\rangle\}$ are the harmonic oscillator number states, $a^\dagger = (\sigma^{-1/2}\hat{q} - \imath\sigma^{1/2}\hat{p})/(\sqrt{2\hbar})$, and $z = (\sigma^{-1/2}q - \imath\sigma^{1/2}p)/(\sqrt{2\hbar})$ with $\sigma > 0$. Note that $\langle z|z\rangle = 1$ while $\langle z|z'\rangle \neq 0$. Written explicitly for $1-$ degree of freedom,

$$\langle x|z\rangle = \left(\frac{1}{2\pi(\Delta q)^2}\right)^{1/4} e^{ipx-(x-q)^2/4(\Delta q)^2}, \tag{12}$$

which is the minimum uncertainty wave packet whose Wigner transform is the Gaussian used in Eq. (8).

From Eq. (10), it is evident that ρ_h takes only positive values. The minimum wave packets, $|z\rangle$ and $\langle z|$ are eigenfunctions of $\hat{a}$ and $\hat{a}^\dagger$, respectively, with eigenvalues z and z^*. Equation (10) follows directly from Eqs. (2) and (4) using the expansion of the identity operator

$$\hat{I} = \int d\mu(z)|z\rangle\langle z|, \tag{13}$$

where $d\mu(z) = dqdp/(2\pi\hbar)$.

If the system under consideration is ergodic, the Husimi density $\{\rho_h^n\}$, corresponding to a sequence of eigenstates $\{\psi_n(q)\}$ with eigenvalues $E_n \to E$, almost always converges to the classical Liouville measure μ_E over the energy surface Σ_E. Thus, if $f(q,p)$ is any smooth observable,

$$\int f(q,p)\rho_h^n dqdp \to \int_{\Sigma_E} f(q,p)d\mu_E \quad \text{as} \quad E \to E_n. \tag{14}$$

Schnirelman's theorem, however, allows an occasional exception (e.g., scarred state) and for this reason, a more appropriate description of nonintegrable eigenfunctions is desirable.

In 1990, Leboeuf and Voros [9] proposed that the zeros of the Husimi function provide a minimal description of quantum states [10]. The first step in this direction is the coherent state $(\sigma = 1)$ or Bargman representation, $\langle z|\psi\rangle$ of a state $|\psi\rangle$ which maps unitarily the standard Hilbert space onto the space of *entire* functions with finite Bargman norm:

$$\|\psi\| = \frac{1}{2\pi\hbar}\int_{R^2}|\psi(z)|^2 e^{-|z|^2}dqdp. \tag{15}$$

One can thus consider $\psi(z)$ as a phase-phase representation of the wave vector $|\psi\rangle$. Note that the zeros of the Bargman and Husimi functions are identical. The Bargman function, however, contains information about the phase (of the wave function) as well and is hence a more fundamental object. For the standard case when the phase space is a plane (the Weyl-Heisenberg group W_1),

$$\psi(z)=e^{-|z|^2/2}\sum_{n=0}^{\infty}\frac{a_n}{\sqrt{n!}}z^n \quad (W_1), \tag{16}$$

where a_n are the expansion coefficients of $|\psi\rangle$ in terms of the harmonic oscillator number states. Similar results can be written down for the sphere [SU(2)] and the pseudo-sphere [SU(1,1)] [12,13], though unlike the case of W_1 or SU(1,1), the Bargman representation of $|\psi\rangle$ for SU(2) is finite, reflecting the compactness of phase space. For Hamiltonian systems, however, energy conservation does ensure that the manifold is compact so that Eq. (16) has, in practice, only a finite number of terms. Clearly, then, the Husimi-Bargman zeros specify a state completely.

It is evident that the distribution of the Husimi-Bargman zeros depends on the distribution of the expansion coefficients $\vec{a}=(a_1,a_2,\ldots,a_n)$. For chaotic systems, it is natural to expect that the choice of an arbitrary basis (harmonic oscillator in this case) makes $\vec{a}$ point in any direction of Hilbert space with equal probability [13]. The only constraint then comes from normalization so that $\Sigma a_n^2=1$. For purposes of computing the distribution of zeros, this is equivalent to the assumption that the coefficients are drawn from a Gaussian distribution [14]:

$$D(\vec{a})=\frac{1}{(2\pi)^N}\exp\left(-\sum_i\frac{|a_i|^2}{2}\right). \tag{17}$$

Equation (16) with the above distribution is referred to as a *random analytic function*.

Random analytic functions (RAF's) for various groups have been studied in some detail when the coefficients are complex [13,15–17] corresponding to systems without time reversal symmetry. The results point to a universal behavior. Thus, the density of zeros is uniform with spacings of the order of $1/\sqrt{N}$ and the two-point correlation has a simple form [17,18] independent of the location of the zeros. Importantly, random analytic functions do seem to model chaotic systems very well [16,19].

For RAF's with real coefficients (systems with time reversal symmetry), Prosen [20] has studied the density and the k-point correlations. The density in this case is nonuniform due to the presence of zeros on the symmetry axis (the real line). Away from the real axis, however, the density becomes uniform, and in this region, correlations tend towards the case with complex coefficients. There are few numerical studies, however, on chaotic systems with time reversal symmetry though it might be expected that RAF's with real coefficients do model them rather well.

In contrast, it is known [21] that for integrable systems, eigenfunctions follow a WKB-type ansatz [see Eq. (1)] in the Bargmann representation too, from which it follows that the zeros lie on fixed curves which are anti-Stokes lines of the complex classical action in the z variable, along which the zeros are equispaced with separation of order $1/N$.

For the sake of completeness, it may also be noted that a random polynomial

$$\psi(z)=a_0+a_1z+a_2z^2+\cdots+a_Nz^N, \tag{18}$$

with coefficients distributed according to Eq. (17), has zeros which tend to accumulate around the unit circle [15].

With this background, we shall explore the distribution of Husimi zeros for polygonal billiard eigenfunctions in the following sections. Unless otherwise stated, we shall consider enclosures with unit perimeter and $\sigma=1$ (coherent state). We shall also consider the energy, $E=1$, and instead quantize $\hbar$ so that $\hbar=1/k$. The $\hbar\to 0$ then corresponds to the classical dynamics at $E=1$.

III. POLYGONAL BILLIARDS AND THE QUANTUM MAP

Classical billiards are enclosures within which a point particle undergoes specular reflection. The dynamics thus depends on its shape. For rational polygonal enclosures, the dynamics is constrained by two constants of motion such that the invariant surface is two dimensional. For the rectangle and the integrable triangles, this is a torus for which $g=1$. For all other rational polygons, the invariant surface is topologically equivalent to a sphere with multiple holes ($g>1$). The simplest example is a double torus ($g=2$) which corresponds to enclosures such as the $\pi/3$ rhombus or the L-shaped billiard. In general, the genus of any rational polygon can be calculated from its interior angles. Thus, if $m_i\pi/n_i$ are the interior angles of a rational polygon,

$$g=1+\frac{N}{2}\sum_i\frac{m_i-1}{n_i}, \tag{19}$$

where N is the least common multiple of n_i, so that the number of sheets that constitute the invariant surface is $2N$. Thus various sets of internal angles may have the same genus but with different N such that the number of distinct momenta spanned by a generic trajectory varies from enclosure to enclosure.

While the genus does affect certain classical features of the system [22], its influence on quantum states is not known for certain. Studies on irrational and rational rhombus billiards show that there is little difference between the morphologies of generic eigenfunctions or their Husimi densities [23]. Shudo and Shimizu [23] even note that "... the difference between random features of eigenfunctions of quantum polygonal and the desymmetrized dispersing system are minute ...." The only difference, they noted, was the occurrence of bouncing ball states though these can be observed in other chaotic systems such as the stadium billiard.

Our investigation of polygonal billiard eigenfunctions lies in this backdrop. Instead of the Husimi densities themselves, we shall study their zeros following Tualle and Voros [1]. The systems we choose are triangles and rhombus billiards, and for all practical purposes, these can be treated as pseudo-integrable systems irrespective of the internal angle [24,25].

The eigenvalues and eigenfunctions can be obtained by solving the Helmholtz equation

$$(\nabla^2+E)\Psi(q)=0, \tag{20}$$

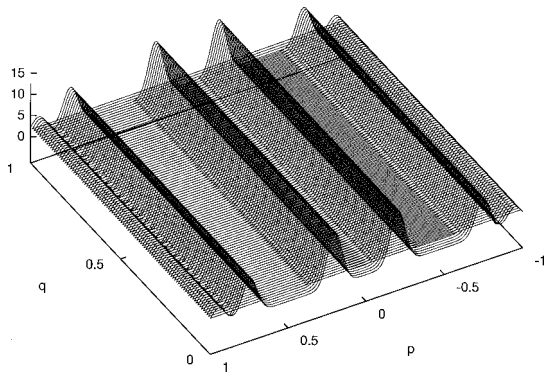

FIG. 1. The z axis is the Husimi density ρ_h of the equilateral triangle eigenfunction at $k=900.142$ corresponding to the quantum numbers (26,81).

with $\Psi(q)=0$ on the boundary. The problem can, however, be reduced to an eigenvalue problem for an integral operator K or a *quantum Poincaré map* in various ways [26]:

$$\psi(s)=\oint ds'\,\psi(s')K_D(s,s';k), \tag{21}$$

$$K_D(s,s';k)=-\frac{\imath k}{2}\cos\theta(s,s')H_1^{(1)}(k|\vec{s}-\vec{s}'|), \tag{22}$$

$$\cos\theta(s,s')=\hat{n}(\vec{s})\cdot\hat{\rho}(s,s'), \tag{23}$$

where $E=k^2$, $\hat{\rho}(s,s')=(\vec{s}-\vec{s}')/|\vec{s}-\vec{s}'|$, and $\hat{n}(\vec{s})$ is the outward normal at the point $\vec{s}$. The unknown function is now the normal derivative on the boundary

$$\psi(s)=\hat{n}(\vec{s})\cdot\nabla\Psi(\vec{s}), \tag{24}$$

and the full interior eigenfunction can be recovered through the mapping

$$\Psi(q)=-\frac{\imath}{4}\oint ds H_0^{(1)}(k|\vec{s}-\vec{s}'|)\psi(s). \tag{25}$$

Thus, the essential dynamical information lies within the reduced $1-d$ function $\psi(q)$ and we shall use this to study phase-space representations and look at their zeros. For an enclosure of unit perimeter (which we shall assume from now on), $\psi(q+1)=\psi(q)$. The Bargman transform $\psi(z)$ thus obeys a quasiperiodicity condition as well [1],

$$\psi(z+1)=e^{(i/\hbar)p}\psi(z), \tag{26}$$

and the norm-finiteness condition becomes

$$\|\psi\|=\frac{1}{2\pi\hbar}\int_{-\infty}^{+\infty}dp\int_0^1 dq|\psi(z)|^2e^{-|z|^2}<\infty. \tag{27}$$

IV. HUSIMI ZEROS IN POLYGONS: RESULTS

The distribution of Husimi-Bargman zeros in polygonal billiards has not been investigated before, and as remarked earlier, the only properties known about the eigenfunctions are from numerical studies. The lack of concrete results leaves us with little expectation and perhaps the only conjecture that can be made is that the distribution of Husimi zeros of polygonal billiards should differ from the regularly spaced

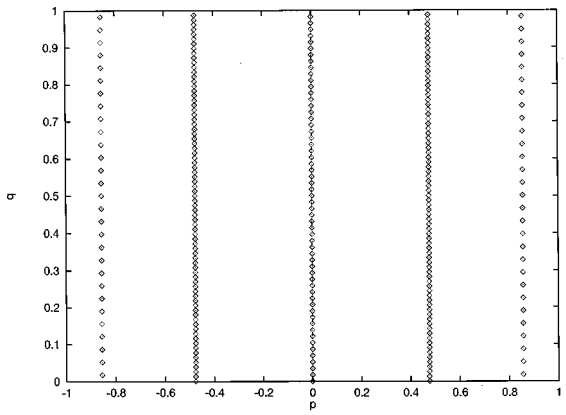

FIG. 2. Husimi zeros of the eigenfunction considered in Fig. 1.

zeros along fixed curves typical of integrable systems.

Note that classical Poincaré section plots in suitable (Birkhoff) coordinates do not immediately reveal the dramatic difference between integrable and pseudointegrable polygons. In both cases, the points lie along a finite number of $\sin\theta$=constant lines where θ is the angle between the ray and the inward normal at the boundary point q. Thus there is little difference between the Poincaré sections of the equilateral triangle and the $\pi/3$ rhombus. With increasing genus, however, the number of such lines generally increases as the trajectory explores a larger number of momentum directions.

Semiclassically, the Husimi eigendistribution function is known to be localized near the torus for integrable systems [27] while its zeros distribute themselves along curves maximally distant from the invariant curves (anti-Stokes lines). As an example, we first consider the equilateral triangle billiard. Figure 1 shows the Husimi distribution of a typical eigenstate with quantum number $(m,n)=(26,81)$ while Fig. 2 is a plot of its zeros. Clearly, the Husimi distribution is peaked on the corresponding torus as evident from Fig. 3 while the zeros lie on lines located away from the torus. Further, the zeros are equispaced on each line though the spacings typically do vary from line to line.

The zeros do not always distribute themselves along straight lines in all integrable polygons and the equilateral triangle with its high symmetry is a rather special case. In

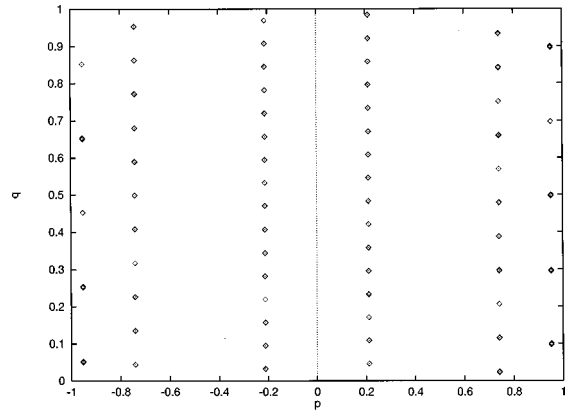

FIG. 3. Classical surface of the section plot in Birkhoff coordinates of trajectories on the corresponding torus (see Fig. 1 for details). Here $p=\sin\theta$ where θ is the angle between the ray and the inward normal at the point q measured along the boundary.

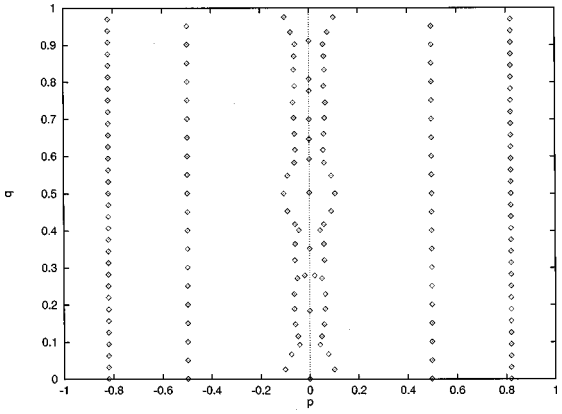

FIG. 4. Husimi zeros of the equilateral triangle mode at $k = 532.751$ viewed in the $\pi/3$ rhombus.

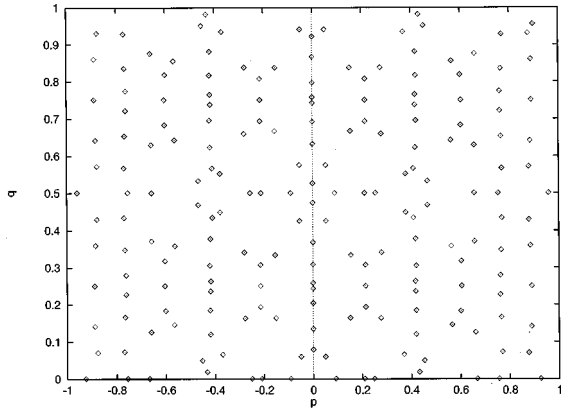

FIG. 6. Zeroes of a neighboring bouncing-ball ''pure rhombus'' mode at $k = 660.531$.

fact, the distribution of zeros of an equilateral state viewed in another enclosure [related by symmetry—for instance, the $(\pi/6,\pi/3,\pi/2)$ triangle or the $\pi/3$ rhombus] looks very different. Figure 4 is an example where the fixed curves are not always straight lines though the zeros are equispaced along each curve.

As examples of pseudointegrable polygons, we shall consider rhombus and triangle billiards. Since the choice of enclosure plays an important role in determining the distribution of zeros, we shall use the $\pi/3$ rhombus to compare the regular and irregular states. Note that the regular states in this case correspond to equilateral triangle modes which vanish on the shorter diagonal and they comprise approximately half the total number of states in the $\pi/3$ enclosure (Fig. 4 is an example). The irregular states, on the other hand are ''pure rhombus'' modes [7] which do not vanish on the shorter diagonal. Barring the bouncing-ball modes, ''pure rhombus'' modes display features typical of irregular wave functions. We shall look for the differences in the distribution of zeros between (i) regular and irregular modes and (ii) bouncing-ball and nonbouncing-ball ''pure rhombus'' modes.

Figure 5 displays the zeros of a typical irregular ''pure rhombus'' mode. The zeros are no longer distributed along curves and they tend to diffuse all over the phase space. Note that there is a reflection symmetry in this case about the $q = 0.25$, 0.5, and 0.75 lines; so the zeros need only be viewed in a quarter of the phase space. Clearly, they are more or less randomly distributed with no clear alignment along any curve, barring some exceptions where two or more zeros are distributed around some $p = \text{const}$ line. These observations are in sharp contrast to the distribution of zeros for integrable polygons.

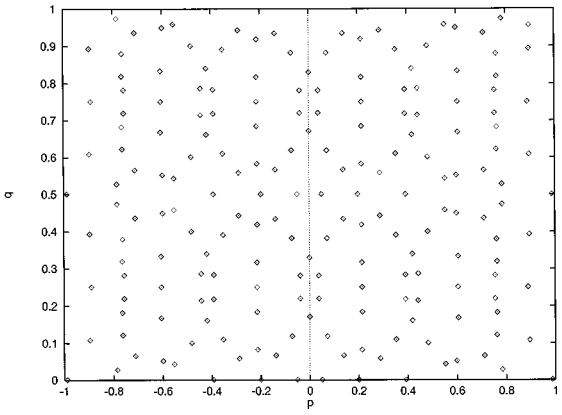

FIG. 5. Zeros of an irregular ''pure rhombus'' mode at $k = 650.336$.

We next look at the zeros of a neighboring bouncing-ball state. Studies on the stadium billiard have shown that the Husimi zeros of bouncing-ball modes are distributed randomly over the entire phase space as in case of irregular modes—an observation that may seem counterintuitive, keeping in mind the existence of approximate quantum numbers in the description of such states [28]. Figure 6 shows the Husimi zeros of a typical bouncing-ball mode in the $\pi/3$ rhombus. The distribution is no different from the earlier case with few zeros distributed around $p = \text{const}$ lines and the other zeros distributed randomly.

The symmetry of the rhombus leads to redundant zeros and hence poor statistics as compared to an unsymmetric polygon at the same energy. However, it does show that the Husimi zeros do not align themselves along fixed curves but rather tend to diffuse over phase space with some amount of clustering around a few $p = \text{const}$ lines. As further evidence, we display the Husimi zeros of a typical state in the $(\pi/4,\pi/5)$ triangle in Fig. 7. They are indeed distributed over the entire classical phase space while the dashed lines indicate a tendency to cluster around certain momenta. This effect, however, seems to be pronounced only in systems with low genus. Thus, for the triangle with internal angles $(97\pi/301,79\pi/501)$, there seems to be little or no clustering (see Fig. 8) and the zeros seem to be genuinely distributed over the entire phase space as in chaotic billiards. Figure 9 shows a set of four histograms which illustrate this difference in clustering. The x axis of the histograms gives the momenta value and the y axis shows the fraction of zeros occurring in a bin. The peaked distribution at specific p values for the low-genus $(\pi/4,\pi/5)$ triangle indicates a clustering of its zeros. In contrast the high-genus case shows an almost uniform distribution of zeros away from the real axis marked by a nearly flat histogram (barring the enhanced density around $p = 0$).

Thus, eigenstates of generic [25] pseudointegrable billiards tend to behave like their chaotic counterparts insofar as the distribution of zeros is concerned. This suggests that

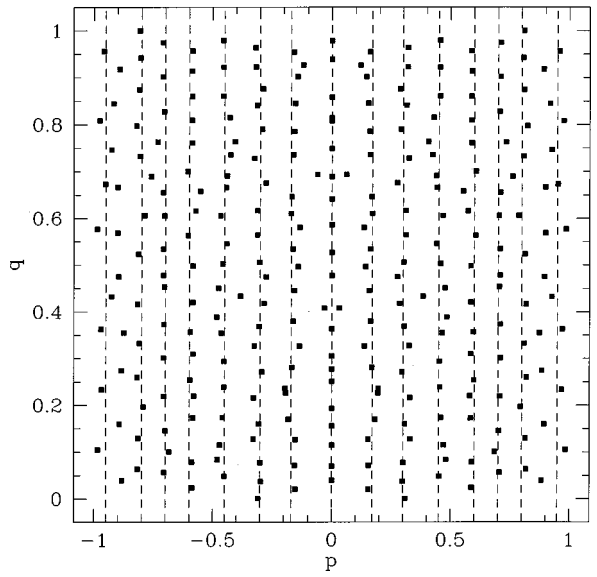

FIG. 7. Husimi zeros of the $(\pi/4, \pi/5)$ triangle mode at 900.239. The dashed lines indicate constant p lines about which some zeros have a tendency to cluster.

there is no obvious semiclassical correspondence in nonintegrable polygonal billiards. In integrable polygons, however, the correspondence is clear at least when $\Delta q_i = \Delta p_i = \sqrt{\hbar/2}$ [see Eq. (9)]. However, when this not so (the minimum uncertainty state is not a coherent state [29]), the zeros tend to move with σ. As an example, we display here the zeros of an equilateral triangle mode for two values of σ in Fig. 10. When $\sigma = \sqrt{\hbar/2}$, the zeros are equispaced and lie on a line. However, as σ is reduced, the zeros move outwards and realign themselves on a curve as shown in the figure. Finally, as σ is reduced further, the zeros start moving out of the classical phase space.

V. CORRELATIONS

In the previous section, we found that the zeros in nonintegrable polygonal enclosures are uniformly distributed away from the real axis and hence are like those of random analytic functions with real coefficients which presumably model chaotic systems with time reversal symmetry. To ascertain how close the distributions are, we shall study here the nearest-neighbor spacing distribution $P(s)$ and the two-point correlation $R_2(r)$.

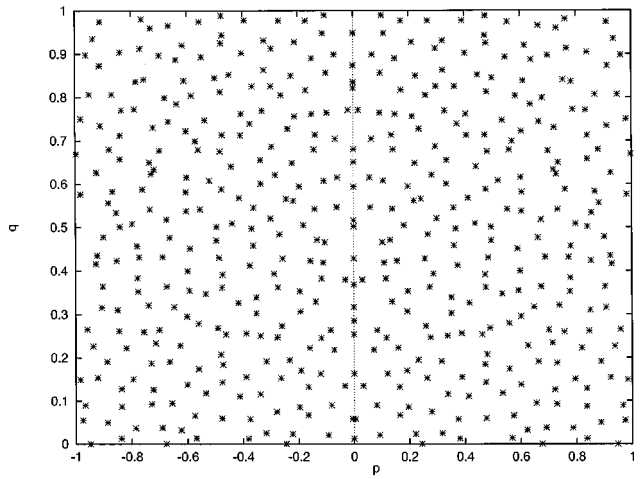

FIG. 8. Husimi zeros of the $(97\pi/301, 79\pi/501)$ triangle for which $g \gg 1$. The distribution is similar to those of chaotic billiards even though the invariant surface is two-dimensional. Here $k = 1500.1803$.

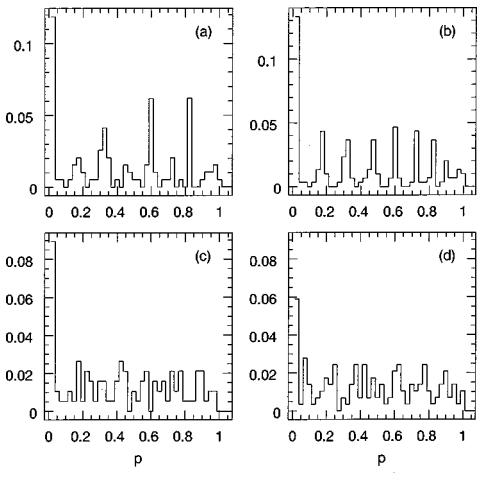

FIG. 9. Histograms illustrating the clustering of zeros. The x axis gives the value of momenta p ($p \in [0,1]$ is shown; the interval $p \in [-1,0]$ is a reflection of $[0,1]$). The y axis of the histogram shows the fraction of zeros occurring in a bin around p. Here bin size is 0.025. Four cases are shown: (a) zeros of the $(\pi/4, \pi/5)$ triangle mode at 600.099, (b) zeros of the $(\pi/4, \pi/5)$ triangle mode at 900.239, (c) zeros of the $(12345\pi/89762, 2011\pi/5431)$ triangle at 600.125, and (d) zeros of the $(12345\pi/89762, 2011\pi/5431)$ triangle at 900.071. The peaked distribution at specific p values for the low-genus $(\pi/4, \pi/5)$ triangle indicates a clustering of its zeros. In constrast the high genus case shows an almost uniform distribution of zeros marked by a nearly flat histogram (barring the enhanced density around $p = 0$).

A. Nearest-neighbor distribution

The nearest-neighbor spacings distribution is the simplest statistic to perform though there exists no analytic predictions for RAF's with real or complex coefficients. The curve in Fig. 11 for random analytic functions is thus determined

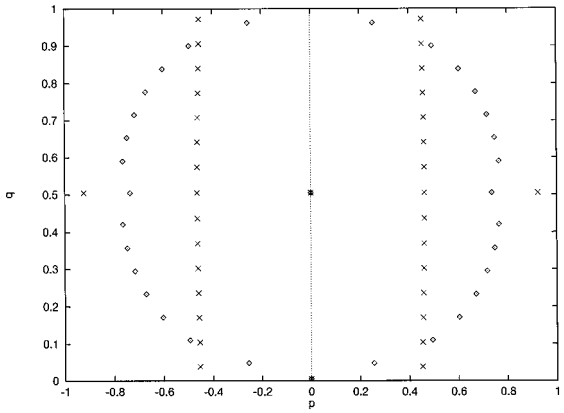

FIG. 10. Two sets of zeros for $\Delta q = \sqrt{\hbar/2} = 0.064\,583\,2$ ($\times$) and 0.018 ($\diamond$), respectively, for an equilateral state. Notice the zeros moving away in the latter case. As Δq is reduced further, some of the zeros leave the classical phase space.

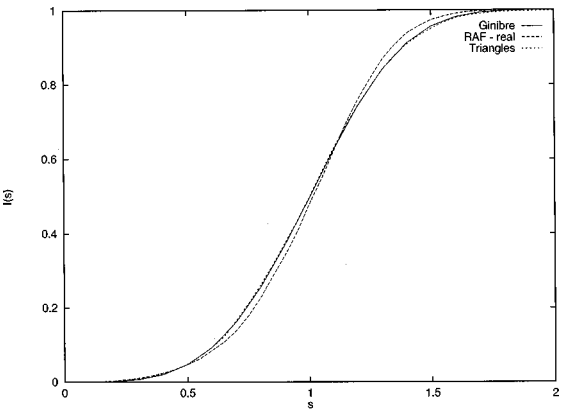

FIG. 11. The integrated nearest-neighbor distribution $I(s) = \int_0^s P(s')ds'$ for (i) nonintegrable triangles (short-dashed curve), (ii) Gaussian random analytic function with real coefficients (long-dashed curve), and (iii) the prediction for the Ginibre ensemble of complex matrices (solid line).

numerically. A total of approximately 25 000 zeros from 50 eigenstates of three different nonintegrable triangles has been used for computing the nearest-neighbor distribution of generic polygons. The zeros have been unfolded such that $\int sP(s)ds = 1$

Figure 11 shows a plot of the integrated spacing distribution $I(s) = \int_0^s P(s')ds'$ for polygons and a comparison with random analytic function having real coefficients. The agreement is fair but there are deviations indicating perhaps that the underlying assumption about the distribution of coefficients [see Eq. (17)] is not fully justified.

Remarkably, however, the Ginibre ensemble [30,31] of complex random matrices shows much better agreement as is evident from Fig. 11. In this case, the integrated spacing distribution [31] $I_G(s) = i(\langle s \rangle s)$ where $\langle s \rangle = \int_0^\infty ds[1 - i(s)] = 1.142\,929$ and

$$i(s) = 1 - \lim_{N\to\infty} \prod_{n=1}^{N-1} [e_n(s^2)e^{-s^2}], \tag{28}$$

where

$$e_n(x) = 1 + \frac{x}{1!} + \frac{x^2}{2!} + \cdots + \frac{x^n}{n!}. \tag{29}$$

At small values of s, $I_G(s) \sim s^4$ and hence $P(s) \sim s^3$. In comparison, the nearest neighbor spacing distribution for uncorrelated points thrown at random on the plane exhibits no level repulsion.

B. Two-point correlation

For SU(2) random analytic functions with complex coefficients, the k-point correlation function has been computed by Hannay analytically. In particular, the two-point function $R_2(\mathbf{r}_1, \mathbf{r}_2) = \langle \rho(\mathbf{r}_1)\rho(\mathbf{r}_2) \rangle$ depends only on the relative distance r between points $\mathbf{r}_1$ and $\mathbf{r}_2$ since the density if uniform. In the asymptotic (number of zeros, $N \to \infty$) limit,

$$R_2(r) \simeq \frac{(\sinh^2 v + v^2)\cosh v - 2v \sinh v}{\sinh^3 v}, \tag{30}$$

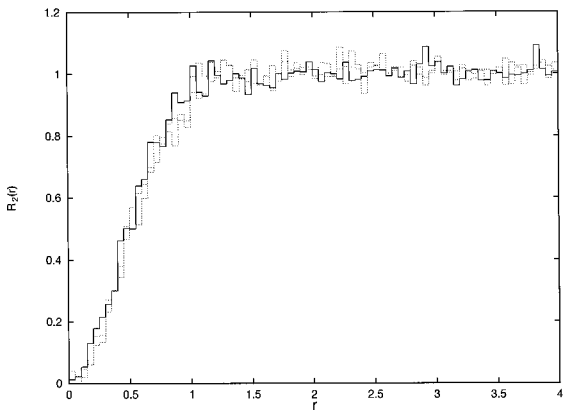

FIG. 12. The two-point correlation R_2 for three different nonintegrable triangles $(8\pi/31, 17\pi/97)$, $(97\pi/301, 79\pi/501)$, and $(12345\pi/89762, 2011\pi/5431)$. Here r is measured in terms of the mean spacing $\sqrt{2\pi\hbar}$.

where $v = \pi r^2/2$ and r is measured in terms of the mean spacing ($\sqrt{4\pi/N}$ for the sphere). This result holds for other phase-space topologies as well when $N \to \infty$ and the coefficients are complex.

For systems with time reversal symmetry (real coefficients), the density is not uniform everywhere and hence $R_2(\mathbf{r}_1, \mathbf{r}_2)$ is sensitive to the location of the zeros. Away from the real axis, however, R_2 has the limiting behavior given by Eq. (30).

For the Ginibre ensemble of complex random matrices, the density is uniform and the two-point correlation (in unfolded units)

$$R_2(\mathbf{r}_1, \mathbf{r}_2) = 1 - \exp(-\pi |r_1 - r_2|^2) \tag{31}$$

is a function of the distance between the two zeros. Note that Eq. (31) does not have the characteristic hump at $r \simeq 1$ associated with random analytic functions.

In Fig. 12, we present results for three different triangles. The close agreement suggests that there is possibly a universality in the distribution of zeros of nonintegrable polygons (corroborated by similar studies on the nearest neighbor). We next compare (see Fig. 13) the average of the combined data with the predictions for the Ginibre ensemble [see Eq. (31)]

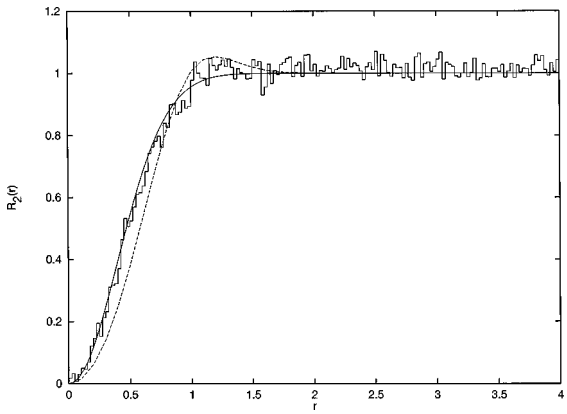

FIG. 13. The two-point correlation R_2 averaged over the three triangles (histogram) compared to the prediction for Gaussian random analytic functions with complex coefficients (dashed curve) and the Ginibre ensemble prediction [solid curve; see Eq. (31)].

and Eq. (30). The deviations from the RAF predictions [32] are evident while the Ginibre ensemble result agrees with our data very well.

VI. CONCLUSIONS

We have studied the distribution of Husimi zeros in polygonal billiards in this paper and our observations can be summarized as follows.

(i) In integrable enclosures, the Husimi density is peaked on the classical torus and the zeros lie equispaced on fixed curves that are located away from the torus when the minimum uncertainty state is a coherent state.

(ii) The zeros tend to move as the uncertainties in position and momentum are varied even as they obey the minimum uncertainty relation. Thus, coherent states ($\Delta p = \Delta q = \sqrt{\hbar/2}$) are the most classical of all minimum uncertainty states.

(iii) A weak signature of pseudointegrability can be associated with the clustering of some zeros around a few lines as observed in some low-genus polygons.

(iv) For generic pseudointegrable enclosures, the zeros tend to be randomly distributed over the entire phase space as in chaotic billiards or random analytic functions with real coefficients. This is especially true for polygons with high genus.

(v) The nearest-neighbor spacing distribution of zeros and the two-point correlation $R_2(r)$ suggests that for pseudointegrable billiards, the correlations are very well described by the Ginibre ensemble of complex random matrices. It is, however, not clear why this is so and a proper understanding is desirable.

ACKNOWLEDGMENTS

The authors acknowledge stimulating discussions with Professor A. Voros and thank Dr. Pragya Shukla for valuable help in our studies on correlations. D.B. also acknowledges several useful discussions on quasiprobability distributions with Dr. R. R. Puri.

[1] J.-M. Tualle and A. Voros, Chaos Solitons Fractals **5**, 1095 (1995).
[2] P. Leboeuf and A. Voros, in *Quantum Chaos: Between order and disorder*, edited by G. Casati and B. V. Chirikov (Cambridge University Press, Cambridge, England, 1995), p. 507.
[3] P. J. Richens and M. V. Berry, Physica D **2**, 495 (1981).
[4] J. B. Keller and S. I. Rubinow, Ann. Phys. (N.Y.) **9**, 24 (1960).
[5] A. Schnirelman, Usp. Mat. Nauk **29**, 181 (1974).
[6] V. N. Prigodin, N. Taniguchi, A. Kudrolli, V. Kidambi, and S. Sridhar, Phys. Rev. Lett. **75**, 2392 (1995), and references therein.
[7] D. Biswas and S. R. Jain, Phys. Rev. A **42**, 3170 (1990).
[8] See, for instance, W. Zhang, D. Feng, and R. Gilmore, Rev. Mod. Phys. **62**, 867 (1990).
[9] P. Leboeuf and A. Voros, J. Phys. A **23**, 1765 (1990).
[10] More recently, Nonnenmacher and Voros [11] have rigorously established that the semiclassical convergence of the Husimi densities towards the uniform ergodic measure implies the equidistribution of the corresponding zeros over the phase space in the classical limit.
[11] S. Nonnemacher and A. Voros, e-print chao-dyn/9711016.
[12] A. M. Perelomov, Usp. Fiz. Nauk **123**, 23 (1977) [Sov. Phys. Usp. **20**, 703 (1977)].
[13] P. Leboeuf, e-print chao-dyn/9901019.
[14] M. Kac, *Probability and Related Topics in Physical Sciences* (Interscience, New York, 1959).
[15] E. Bogomolny, O. Bohigas, and P. Leboeuf, J. Stat. Phys. **85**, 639 (1996).
[16] P. Leboeuf and P. Shukla, J. Phys. A **29**, 4827 (1996).
[17] J. H. Hannay, J. Phys. A **29**, L101 (1996).
[18] In [17], Hannay has derived a general expression for the *k*-point correlation function.
[19] P. Shukla, J. Phys. A **30**, 6313 (1997).
[20] T. Prosen, J. Phys. A **29**, 4417 (1996).
[21] A. Voros, Phys. Rev. A **40**, 6814 (1989).
[22] D. Biswas, Pramana, J. Phys. **48**, 487 (1997).
[23] A. Shudo and Y. Shimizu, Chaos Solitons Fractals **5**, 1137 (1995).
[24] Irrational billiards are conjectured to be ergodic—see, for example, A. Hobson, J. Math. Phys. **16**, 2210 (1976); R. Artuso, G. Casati, and I. Guarneri, Phys. Rev. E **55**, 6384 (1997).
[25] For computational purposes, irrational polygons are systems with high genus.
[26] P. A. Boasman, Ph.D. thesis, University of Bristol, U.K., 1992 (unpublished).
[27] K. Takahashi, J. Neurophysiol. **55**, 762 (1986).
[28] Y. Y. Bai, G. Hose, K. Stefański, and H. S. Taylor, Phys. Rev. A **31**, 2821 (1985).
[29] R. J. Glauber, Phys. Rev. **131**, 2766 (1963); R. R. Puri, Pramana, J. Phys. **48**, 787 (1997).
[30] M. L. Mehta, *Random Matrices* (Academic, New York, 1991).
[31] R. Grobe, F. Haake, and H-J. Sommers, Phys. Rev. Lett. **61**, 1899 (1988).
[32] Note that in Figs. 11 and 13, no attempt has been made to separate the zeros close to and far away from the real axis for either the RAF result on $I(s)$ or the polygonal billiard results on $I(s)$ and $R_2(r)$. The effect of nonuniformity has, however, been found to be small for the number of zeros considered.